Dalton Transactions

PAPER

View Article Online
View Journal | View Issue

Cite this: *Dalton Trans.*, 2015, **44**, 10817

High temperature neutron diffraction studies of $PrInO_3$ and the measures of perovskite structure distortion

A. Baszczuk,*[a] B. Dabrowski[b] and M. Avdeev[c]

Received 16th December 2014,
Accepted 27th February 2015

DOI: 10.1039/c4dt03881a

www.rsc.org/dalton

The crystal structure of $PrInO_3$ was investigated in the temperature range 303–1123 K by high-resolution neutron-powder diffraction. The $PrInO_3$ adopts a highly distorted variant of the perovskite structure with the orthorhombic *Pnma* space group in the whole temperature range investigated. The bond length and bond-angle analysis revealed a very slow tendency to decrease structural distortion with increasing temperature. Comparison of different parameters quantifying perovskite structure distortion calculated for $PrInO_3$ and the similar $PrAlO_3$ and $PrGaO_3$ shows the advantage of using the tolerance factor t_{12} calculated for the 12-fold coordinated Pr by geometrical averaging of the individual interatomic distances. An additional advantage of the tolerance factor method results from the possibility of extending it to predict the average structural distortion and the geometrical stability of the perovskites at various temperatures once the accurate dependence of $t(x,T,d)$ on the composition, temperature and oxygen content is found. By comparing $PrInO_3$ with several AMO_3 perovskites containing ions in the fixed oxidation state on the A and M crystal sites it was found that structural distortion and the tolerance factor t_{12} for $PrInO_3$ are consistent with the empirical thermal expansion coefficient based on the bond strength calculation [R. M. Hazen, and C. T. Prewitt, *Am. Mineral.*, 1977, **62**(3–4), 309]. In contrast to perovskites AMO_{3-d} containing mixed-valent M ions, which allow for a wide range of changes of the tolerance factor $t_{12}(T,d)$ as a function of oxygen content, perovskites AMO_3 with M ions in the fixed oxidation state show much less flexibility. This flexibility is further reduced for the $A^{3+}M^{3+}O_3$ perovskites like $PrInO_3$ for which even a large change of the synthesis temperature has a minor effect on controlling the resulting $t_{12}(T)$ and the structural phase in comparison with $A^{2+}M^{4+}O_3$ perovskites. The only parameter left for $A^{3+}M^{3+}O_3$ materials allowing formation of various perovskites and hexagonal phases is the total pressure, which may significantly change $t_{12}(T,P)$.

Introduction

Rare earth (R) and alkaline earth (A) transition-metal (M) perovskites (R/A)MO_3 exhibit a wide range of exceptional properties (electronic, superconducting, magnetic, dielectric, optical, *etc.*) and therefore are researched in several useful fields including solid oxide fuel cells, multiferroics, ferromagnets, magnetotransport, and photoluminescence to name a few.[1,2] Perovskites containing metal M from the p-block of the periodic table are equally useful; for example, aluminates and gallates are widely used as substrate materials for the epitaxy of the superconducting cuprates, magnetoresistive materials and semiconducting thin films and multilayers, as scintillators, and electrolytes for solid oxide fuel cells.[3] Recently, a class of materials with the closed shell d^{10} electronic configuration (In^{3+}, Ga^{3+}, Ge^{4+}, Sn^{4+}, and Sb^{5+}) has been investigated in an attempt to develop new photocatalysts for water splitting.[4] Among them the perovskites $RInO_3$ [5] have been reported as the most promising compounds. Considering the valuable physical properties of the transition-metal and post-transition-metal perovskites a much better understanding of their stability at high temperatures is essential for reliable design and synthesis of the desired compositions with improved properties. Previously we have studied several manganites (A/R)MO_{3-d} (M = Mn) for which we observed that it is possible to tune the structural transitions between the perovskite phase, which we define as a network of corner-shared MO_6 octahedra, and the non-perovskite phases such as the hexagonal 4*H* and 2*H* phases with face-shared MO_6 octahedra for large A = Sr and Ba, respectively, and the layered hexagonal $P6_3cm$ phase for

[a]*Wroclaw University of Technology, Department of Mechanics, Materials Science and Engineering, 50-370 Wroclaw, Poland. E-mail: agnieszka.baszczuk@pwr.edu.pl*
[b]*Department of Physics, Northern Illinois University, DeKalb, IL 60115, USA*
[c]*Bragg Institute, Australian Nuclear Science and Technology Organization, Locked Bag 2001, Kirrawee DC, NSW 2232, Australia*

small R = Dy.[6–8] The structural transitions among perovskite and hexagonal phases were relatively easily tunable for manganites by controlling the temperature and oxygen pressure during the synthesis because of the Mn flexible coordination to oxygen and the variable oxidation states of 2+, 3+ and 4+ that affect its ionic size.[9] The stability of the perovskite phase was consistently described in terms of the modified Goldschmidt's tolerance factor $0.855 \leq t(x,T,d) \leq 1$, whose definition was extended to the dependence on the temperature (T) and oxygen content (3-d) that controls the oxidation state of Mn, in addition to the traditional dependence on the chemical composition (x).[10,11] Careful thermogravimetric and neutron diffraction studies were necessary to find the accurate dependence of the mean <A/R–O> and <Mn–O> bond lengths on T and d for deriving reliable $t(x,T,d)$.[6,10,12] The importance of this study for manganites has been demonstrated by proving the predictive capability of $t(x,T,d)$ for the synthesis of new compounds in the (La/Sr/Ba)MnO_3 system.[8,13,14] Once a library of the [A/R–O] and [Mn–O] bond lengths has been achieved, the $t(x,T,d)$ could be found reliably for any (A/R)MnO_{3-d}, and the synthesis conditions might be designed appropriately to stabilize the perovskite phase well beyond the apparent solubility limits, as was recently demonstrated when obtaining a remarkable displacive-type multiferroic $Sr_{0.55}Ba_{0.45}MnO_3$.[15] On the other hand the synthesis conditions could also be designed to destabilize the perovskite phase of, for example, $DyMnO_3$ in favor of the hexagonal $P6_3cm$, which exhibits exceptional oxygen absorption/desorption properties at unusually low temperatures.[7,16]

The similarity of the observed perovskite and layered hexagonal $R\bar{3}c$ phases of $RMnO_3$ to the RMO_3 compounds with the fixed oxidation state M^{3+} = In, Ga, Al motivated us to study and compare these systems by focusing on R = Pr.

In the absence of precise neutron diffraction data the differences observed in the crystal structures of $PrAlO_3$, $PrGaO_3$ and $PrInO_3$ can be evaluated based on the ionic radius of the M ion[9] and the Goldschmidt tolerance factor given by[11]

$$t = \frac{r(\mathrm{Pr}) + r(\mathrm{O})}{\sqrt{2}(r(\mathrm{M}) + r(\mathrm{O}))}$$

where r(Pr), r(O) and r(M) are the radii of the Pr^{3+}, O^{2-} and M^{3+} ions, respectively. The room temperature tolerance factors for $PrAlO_3$, $PrGaO_3$ and $PrInO_3$ are then 0.942, 0.903 and 0.829, respectively, when the ionic radii given by Shannon[9] are used; $r(Pr^{3+})$ = 1.179 Å (for CN = 9), $r(O^{2-})$ = 1.40 Å, $r(Al^{3+})$ = 0.535 Å, $r(Ga^{3+})$ = 0.62 Å and $r(In^{3+})$ = 0.80 Å. From the decrease of $t(x)$ with the increase of the M ionic radii these compounds are expected to exhibit increased distortion of the perovskite crystal structure and the corresponding lowering of symmetry. Indeed this universal relationship was shown[3,17–19] at room temperature where they adopt two different variants of the distorted cubic perovskite structure: rhombohedral symmetry $R\bar{3}c$ for $PrAlO_3$ [17,18] and orthorhombic *Pbnm* (equivalent to *Pnma*) space group for $PrGaO_3$ [3,19] and $PrInO_3$.[20] At elevated temperatures $PrAlO_3$ transforms to the cubic structure at 1770 K.[3,18] Below room temperature $PrAlO_3$ undergoes additional phase transformations to the more distorted structures, orthorhombic at 205 K and monoclinic at 151 K.[21–23] It is believed that these transitions are caused by the electronic effects involving Pr ions, such as the coupling between Pr electronic states and phonons, as well as cooperative Jahn–Teller effects.[23] In contrast to $PrAlO_3$, only one phase transition, namely from $R\bar{3}c$ to *Pbnm*, was observed for the $PrGaO_3$ below 1850 K.[19] To date, as far as we know, studies of the $PrInO_3$ crystal structure are only limited to information about the room temperature unit cell parameters (a = 5.67, b = 5.93, c = 8.18 ± 0.1 Å[20]). Detailed investigation of the $PrInO_3$ structural stability over a wide range of temperatures has become recently important because these materials, as well as the Pr-site substituted compounds, are considered as promising ionic conductors.[24]

While all M = Mn, In, Ga and Al are known to exhibit flexible coordination to oxygen, In, Ga and Al show only the fixed oxidation state 3+, and as such no dependence of the ionic radius on the valence state is observed, which makes it possible to study the dependence of the structural parameters and tolerance factor on the thermal effects alone. In this study the differences observed in thermal expansion of crystal structures, bond-lengths, bond angles and polyhedral distortion of $PrInO_3$ are investigated using neutron powder diffraction (NPD) measurements. The results are compared with $PrAlO_3$ and $PrGaO_3$ in terms of the M-site polyhedral distortion and theory of the bond valence widely applied in solid-state chemistry.[25,26] Precise determination and use of the NPD derived bond-lengths allow one to employ them in place of the sums of the less reliable ionic sizes of r(R/A), r(O) and r(M), and as such, for a much better reliability of the determination of the tolerance factor $t(x,T)$, and prediction of the stability of the desired phases. Comparison of different parameters quantifying perovskite average structural distortion shows that the tolerance factor calculated for the 12-fold coordinated Pr by geometrical averaging of the individual interatomic distances produces the most reliable results, and, in addition, provides the capability of predicting the structural stability and designing new compositions, which are not possible to achieve with the other methods.

Sample preparation and experimental details

The polycrystalline sample $PrInO_3$ was prepared by following the conventional solid-state reaction method. Stoichiometric amounts of high purity (99.999%) Pr_6O_{11} and In_2O_3 oxides were thoroughly mixed in an agate mortar and then pressed into high-density pellets. The sample then underwent several calcination processes in air, with intermediate grinding, in the temperature range of 800–1300 °C followed by natural cooling to room temperature in a furnace. Under these conditions, the single-phase perovskite phase was successfully synthesized.

Neutron powder diffraction data of a polycrystalline sample of $PrInO_3$ were measured between room temperature and

1123 K using the high-resolution powder diffractometer Echidna at ANSTO's OPAL reactor of the Australian Nuclear Science and Technology Organization (ANSTO) using a wavelength of 1.6215 Å. The structures were refined using the Rietveld method with the GSAS (EXPGUI) suite.[27]

Results and discussion

Crystal structure and the measures of the cubic distortion of $PrInO_3$ at room temperature

A preliminary inspection of the NPD patterns obtained for $PrInO_3$ indicated an orthorhombic $GdFeO_3$-type structure with the unit-cell parameters: $a = a_p\sqrt{2}$, $b = 2a_p$ and $c = a_p\sqrt{2}$ (a_p is the ideal cubic perovskite lattice parameter). Throughout this manuscript we will use the standard setting of space group #62, *Pnma*, to describe the crystallography of $PrInO_3$. Although some authors use this setting, many others use the non-standard setting *Pbnm* to describe the perovskites with the $GdFeO_3$ crystal structure.[19] The refinements of the diffraction patterns for $PrInO_3$ carried out in the space group *Pnma* confirmed the validity of this structural model in the whole temperature range (303–1123 K). The final atomic coordinates, lattice parameters and discrepancy factors obtained from structural refinement of the room temperature NPD data are given in Table 1.

Graphical results of the Rietveld refinement for $PrInO_3$ measured at room temperature are shown in Fig. 1. Selected room temperature structural parameters are shown in Table 2.

From the table it is clearly seen that in the distorted structure of $PrInO_3$ the individual Pr–O bonds show very large length differences (~60%) and split into three groups: six short bonds of 2.35–2.69 Å, two medium length bonds of 2.91 Å and four long bonds of 3.47–3.80 Å. A large variation of the bond distances makes the Pr coordination number to oxygen ions uncertain. The octahedral distortion in the orthorhombic $GdFeO_3$-type structure allows for three different doubly degenerate In–O bonds of InO_6, but in contrast to Pr–O bonds, the range of the In–O distances is much smaller.

There are several methods used in the literature in order to define and quantify distortion from the ideal cubic perovskite structure.[11,25,26,28] The observed tolerance factor is probably the most widely used parameter in crystallochemical analysis of $(R/A)MO_3$,[6,10,19,29–33] and is given by

$$t_n = \frac{\langle R/A-O\rangle n}{\sqrt{2}\langle M-O\rangle}$$

where <R/A–O>n and <M–O> are the mean interatomic distances in the polyhedra with the corresponding coordination number n for the (R/A)-site.[28] The tolerance factor provides a measure of how well the R = Pr cation fits into the twelve-fold coordinated space within the corner-shared octahedral network formed by the M-site cations and oxygen. The tolerance factors are usually reported for various coordination of the (R/A)-site cation depending on author's preferences. For severely distorted perovskites coordination very often is reduced from 12 to 9,[29,30] 8[19,31] or even 6 as in the case of $SrCeO_3$.[32] However, it is not obvious when a specific coordination should be used especially when the distortion is gradually changing as a function of temperature or in the solid solution systems. For comparison with the other methods, we calculate here the tolerance factor for severely distorted $PrInO_3$ using the ideal 12-fold and the reduced 8-fold coordinated Pr-sites (see Table 2). Based on the algebraic averaging the interatomic distances are <Pr–O> = 2.9547 Å and <In–O> = 2.1607 Å for the 12- and 6-coordinated Pr and In, respectively. The resulting tolerance factor is close to 1 (t_{12} = 0.97) indicating incorrectly rather low distortion from the ideal cubic perovskite structure. The calculation of the tolerance factor can be improved by the use of the geometrical mean for the 12-co-

Table 1 Crystallographic parameters, atomic positions, thermal parameters, and reliability factors from the Rietveld refinements for $PrInO_3$ at room temperature.[a] Additionally a crystal structure with the two oxygen sites and unit cell axes labeled is shown

Atom	x	y	z	B (Å^2)	Oc.
Pr	0.44176(21)	0.250000	0.48346(27)	0.991(32)	1
In	0	0	0.5	0.655(33)	1
O1	0.55120(19)	0.250000	0.88218(20)	B_{11} = 0.82(5) B_{22} = 0.85(6) B_{33} = 0.728(55) B_{13} = −0.234(39)	1
O2	0.19459(14)	*0.06178(9)*	0.19120(13)	B_{11} = 0.98(4) B_{22} = 1.35(4) B_{33} = 0.882(32) B_{12} = 0.36(4) B_{13} = 0.265(35) B_{23} = 0.10(4)	1

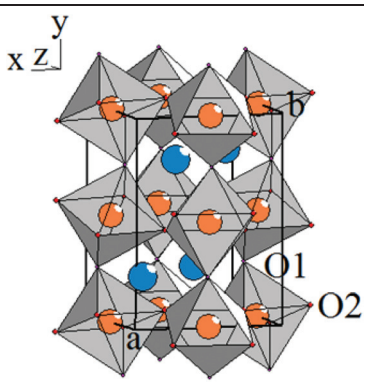

[a] Space group *Pnma*, a = 5.90964(14) Å, b = 8.15432(20) Å, c = 5.66059(13) Å, V = 272.779(17) Å^3. Reliability factors: χ^2 = 1.189, R_{wp} = 2.88%, R_p = 2.25%.

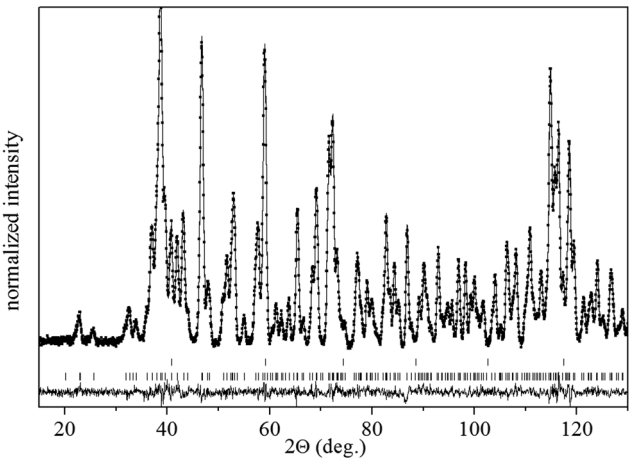

Fig. 1 Rietveld refinement profile for the $PrInO_3$ measured at room temperature. Experimental data points are presented as squares. The solid lines are the refined profile and the difference curve (observed minus refined, plotted at the bottom). Intensity peak positions are marked as short vertical lines for the *Pnma* space group (bottom) and niobium (from furnace heating elements, top).

ordinated Pr-site instead of an algebraic mean. Geometric averaging results in a smaller magnitude of the mean bond <Pr–O> = 2.9041 Å, as it puts less weight on the longer bonds.[6] Geometric averaging of the In–O bonds leads to a virtually identical value as the algebraic mean since the InO_6 octahedra are only slightly distorted. The resulting tolerance factor t_{12} = 0.95 obtained by geometrical averaging expresses much better the large crystal distortion of $PrInO_3$. As will be shown below the t_{12} calculated consistently by using the geometrical means rather than by the use of algebraic means should be more reliable when comparing perovskites with widely varying structural distortion. We will use this method to calculate t_{12} in the following sections to compare the heavily distorted $PrInO_3$ with perovskites with a smaller degree of distortion. From the large Pr–O bond length variation in the orthorhombic $PrInO_3$ it is clear that the smaller coordination number of Pr can also be defined and used. Tolerance factors based on the shorter interatomic distances with 8-coordination for the Pr site are presented in Table 2. The values of t_8 are obviously much smaller than t_{12}. In addition, they are almost the same regardless of the method of averaging because of the way they were selected.

Deviations from the ideal perovskite structure and the magnitude of the polyhedral distortion can be defined in another way by using the so-called bond-length distortion parameter calculated according to the equation:

$$\Delta = \frac{1}{n}\left[\sum_{i}^{n}\left(\frac{d_i - d}{d}\right)^2\right] \times 10^3$$

where d_i and d are, respectively, the individual and average values of the interatomic distances in polyhedra with the coordination number n.[28] We note that as with the tolerance

Table 2 Selected room temperature structural parameters for $PrMO_3$ (M = Al, Ga, In)

Parameters	$PrAlO_3$ [18] $R\bar{3}c$	$PrGaO_3$ [19] *Pbnm*	$PrInO_3$ *Pnma*
Pr–O_1 (Å)	2.442	2.371(2)	2.3478(19)
Pr–O_2 × 2 (Å)	2.442	2.396(1)	2.3592(14)
Pr–O_1 (Å)	2.665	2.509(2)	2.4302(16)
Pr–O_2 × 2 (Å)	2.665	2.619(1)	2.6882(14)
Pr–O_2 × 2 (Å)	2.665	2.727(1)	2.9147(11)
Pr–O_1 (Å)	2.665	3.056(2)	3.4645(20)
Pr–O_1 (Å)	2.891	3.113(2)	3.6810(16)
Pr–O_2 × 2 (Å)	2.891	3.277(1)	3.8044(13)
Algebraic:[a]			
<Pr–O>$_{12}$	2.6658	2.757	2.9547
<Pr–O>$_8$	—	2.546	2.5878
Geometric:[a]			
<Pr–O>$_{12}$	2.6610	2.739	2.9041
<Pr–O>$_8$	—	2.542	2.5777
M–O_2 × 2 (Å)	1.895	1.978(1)	2.1521(7)
M–O_2 × 2 (Å)	1.895	1.984(1)	2.1640(7)
M–O_1 × 2 (Å)	1.895	1.9774(5)	2.1661(4)
Algebraic: <M–O>$_6$ [a]	1.895	1.9798	2.1607
Geometric: <M–O>$_6$ [a]		1.9798	2.1607
M–O_1–M (°)	166.2	155.37(9)	140.48(1)
M–O_2–M × 2 (°)	166.2	155.33(7)	142.89(4)
<M–O–M>	166.2	155.34	142.08
$\cos^2\theta$	0.9431	0.8260	0.6223
Algebraic[b]			
t_{12}	0.9947	0.9848	0.9669
t_8	—	0.9092	0.8469
Geometric			
t_{12}	0.9929	0.9781	0.9504
t_8	—	0.9078	0.8436
Δ(PrO)$_{12}$ [c]	4.1	13.9	35.6
Δ(PrO)$_8$	—	2.9	7.9
Δ(MO)$_6$	0	0.08	0.29

[a] Geometrical and algebraic average bond distances in Pr–O_n (n = 12, 8) and M–O_6 polyhedra. [b] Geometrical and algebraic observed tolerance factors in $PrMO_3$ crystal structures, calculated for reasonable coordination numbers of Pr atoms [c] Bond-length distortion of the Pr–O_n (n = 8, 9, 12) and M–O_6 polyhedra in $PrMO_3$ structures (see the text).

factor calculation, the method of averaging interatomic distances and the selection of n are again loosely defined. The value of $\Delta(InO)_6$ = 0.29 (n = 6, d = 2.1607 Å) is relatively high but much lower than the values of 35.6 and 7.9 obtained for $\Delta(PrO)_{12}$ and $\Delta(PrO)_8$, respectively (see in Table 2), obtained by the algebraic averaging of d for $PrInO_3$.

An alternative method for calculating the valence of the cations and anions present in the solid, which follows Brown's bond-valence model, is also regarded as an excellent method to obtain primary insight into the overall structural stability of perovskites.[25,26] This method gives a phenomenological relationship between the formal valence of a bond and the corresponding bond lengths. In perfect unstrained structures, the bond valence sum (BVS) rule states that the valence (V_{ij}) of the cation (anion) is equal to the sum of the bond valences (v_{ij}) around this cation (anion). Bond valences (bond strengths) are calculated by assuming the exponential formula:

$$v_{ij} = \exp[(R_0 - d_{ij})/0.37],$$

Table 3 Bond valence table for $PrInO_3$ (a), $PrGaO_3$ (b) and $PrAlO_3$ (c). The values have been calculated using the parameter set of Brese and O'Keefe[38]

$PrInO_3$ (a)	O1	$V_{ij\,(calc.)}$	O2	$V_{ij\,(calc.)} \times 2$	$\sum v_{ij}$
Pr	2.3478	0.5672	2.3592 (×2)	1.1000	
	2.4302	0.4540	2.6882 (×2)	0.4521	2.8836
	3.4646	0.0277	2.9147 (×2)	0.2451	
	3.6810	0.0154	3.8044 (×2)	0.0221	
In	2.1661 (×2)	0.9796	2.1521 (×2)	1.0174	2.9822
			2.1640 (×2)	0.9852	
$\sum v_{ij}$	2.0439		1.9110		
GII	0.0770				
$PrGaO_3$ (b)					
Pr	2.371	0.5327	2.396 (×2)	0.9959	
	2.509	0.3669	2.619 (×2)	0.5450	3.0951
	3.056	0.0837	2.727 (×2)	0.4071	
	3.113	0.0717	3.277 (×2)	0.0921	
Ga	1.9774 (×2)	1.0248	1.978 (×2)	1.0231	3.0546
			1.984 (×2)	1.0067	
$\sum v_{ij}$	2.0798		2.0349		
GII	0.0700				
$PrAlO_3$ (c)					
Pr	2.442	0.4397	2.442 (×2)	0.8794	
	2.665	0.2408	2.665 (×2)	0.4813	3.1552
	2.665	0.2407	2.665 (×2)	0.4813	
	2.891	0.1307	2.891 (×2)	0.2613	
Al	1.895 (×2)	1.0343 [0.9511][a]	1.895 (×2)	1.0343 [0.9511][a]	3.1030 [2.8534][a]
			1.895 (×2)	1.0343 [0.9511][a]	
$\sum v_{ij}$	2.0862 [2.003][a]		2.0860 [2.0028][a]		
GII	0.1193/[0.1068][a]				

[a] The values have been calculated using the parameter set of Brown.[39]

where R_0 is the tabulated bond-valence parameter empirically determined for each bond type and d_{ij} is the anion–cation bond length. The valence of the atom i ($V_{i(calc.)}$) is then calculated as $\sum v_{ij}$. No assumption is made about the coordination number of the A-site cation because the valences for twelve A–O bonds are calculated in all cases, but the contribution to the atomic valence sum reduces rapidly with the A–O bond distance increase.

The departure of the BVS rule from formal valence is presumed to measure the existing stress in the bonds for the given structure. The overall stress can be quantified by means of a global instability index (GII) determined by comparing the calculated atomic bond-valence $V_{i(calc.)}$ and the formal valence $V_{i(OX)}$ ($d_i = V_{i(OX)} - V_{i(calc.)}$), from the equation:

$$GII = \left\{ \left[\sum_{i=1}^{N} d_i^2 \right] / N \right\}^{1/2}$$

(N is the number of atoms in the asymmetric unit).[26] Table 3a lists the bond valence sums as well as the GII calculated for Pr, In and O atoms from the individual Pr–O and In–O distances. Bond-valence sums for Pr and In ions within the PrO_9, PrO_{12} and InO_6 coordination polyhedra in $PrInO_3$ are shown in Table 4. In $PrInO_3$, the bond strength sums for Pr^{3+} surrounded by 8, 9, 10 and 12 oxygens are 2.82, 2.85, 2.86 and 2.88, respectively, indicating the dominant bonding of the eight nearest oxygen neighbors. The bond valences of the Pr–O bond length larger than 3.46 Å are smaller than 0.028, and therefore their contribution to the charge balance of the Pr-site is negligible. However, the valence contribution of the

Table 4 Bond valence sums for Pr, M within the PrO_8, PrO_{10}, PrO_{12} and MO_6 coordination polyhedra in $PrMO_3$ (M = Al, Ga, In). The values have been calculated using the parameter set of Brese and O'Keefe[38]

M	$PrAlO_3$	$PrGaO_3$	$PrInO_3$
BV-M(6)	3.10 [2.8534][a]	3.06	2.98
BV-Pr(8)	—	2.85	2.82
BV-Pr(9)	2.76	2.93	2.85
BV-Pr(10)	—	3.00	2.86
BV-Pr(12)	3.16	3.10	2.88
$Pr–O_{(ideal)}$[b]	2.6509	2.6509	2.6509
$M–O_{(ideal)}$	1.9020	1.9865	2.1585
t_{BV}[c]	0.98	0.94	0.87

[a] The value has been calculated using the parameter set of Brown.[39] [b] Ideal Pr–O and M–O bond distances calculated assuming 12 equidistant Pr–O bonds, each contributing a bond valence of $\frac{1}{12}$ of the ideal Pr-site oxidation state and 6 equidistant M–O bonds contributing a bond valence of $\frac{1}{6}$ of the ideal M-site oxidation state (using R_0 parameters given by Brese and O'Keefe[38]). [c] The bond-valence based tolerance factor calculated using ideal Pr–O and M–O bond distances.

two medium Pr–O bonds with a length of 2.9147 Å has a value of 2 × 0.1226, and provides a substantial contribution to the Pr valence, supporting the idea of using simplifying 8-fold coordination for the Pr-site. Nevertheless, irrespective of the chosen coordination number, the Pr cations appear somewhat underbonded indicating that Pr–O bonds are under small tensile stress in $PrInO_3$.

The methods described above to measure the magnitude of perovskite structure distortion require detailed knowledge of all the individual interatomic distances A/R–O and M–O. As such they are "a posteriori" methods usually useful only to verify the validity of the structure refinement of the data obtained preferentially from the NPD measurements. Since the individual interatomic distances A/R–O and M–O cannot be reliably predicted before obtaining new materials these methods are of little help for designing and synthesizing the desired perovskites. However, as shown for manganites the tolerance factor method can be extended to predict the average structural distortion and the geometrical stability of the perovskites at various temperatures once careful thermogravimetric and NPD studies are conducted to find all the necessary mean <A–O>, <R–O>, and <M–O> bond lengths at room temperature and the dependence of $t(x,T,d)$ on the temperature and oxygen content. It is noteworthy to observe that such a study has to be done for each M ion separately since the mean <A/R–O> bonds do not have a universal magnitude, as it could be incorrectly obtained from the tables of ionic radii; for example, $r(^{XII}Sr^{2+}) + r(O^{2-}) = 2.68$ Å,[9] while $[^{XII}Sr–O] = 2.691$ and 2.761 Å for M = Mn[8] and Ti,[34] respectively, for the evidently cubic structures at room temperature.

Thermal dependence of structural properties of $PrInO_3$

Analysis of the $PrInO_3$ cell parameters obtained from NPD data using Rietveld refinement indicated that they increase almost linearly and anisotropically upon heating. Practically, equal relative expansion is observed for the *b* and *c* lattice parameters, whereas the relative expansion along the *a* direction is roughly 2 times lower. Such an anisotropic nature of the thermal expansion of the unit-cell is characteristic also for the other $GdFeO_3$-type orthorhombically distorted perovskites.[3,19,35] The lattice parameter variation is a manifestation of subtle changes in the structural arrangement.

The results of our refinements for the changes of Pr–O interatomic distances with increasing temperature are shown in Fig. 2a. From this figure it could be concluded that all observed Pr–O interatomic distances remain nearly constant in the whole temperature range investigated.

Closer look at Fig. 2a shows that an increase of temperature leads to a slight increase of the short bonds and a decrease of long bonds. Consequently only a slight linear increase of the algebraic and geometric mean <Pr–O> bond lengths calculated using 8 and 12 coordinated Pr is visible (see Fig. 2b). Thermal evolution of individual In–O bonds and their mean are shown in Fig. 2c revealing their slight increases. The resulting tolerance factor variation with increasing temperature calculated using algebraic and geometrical means is shown in Fig. 3.

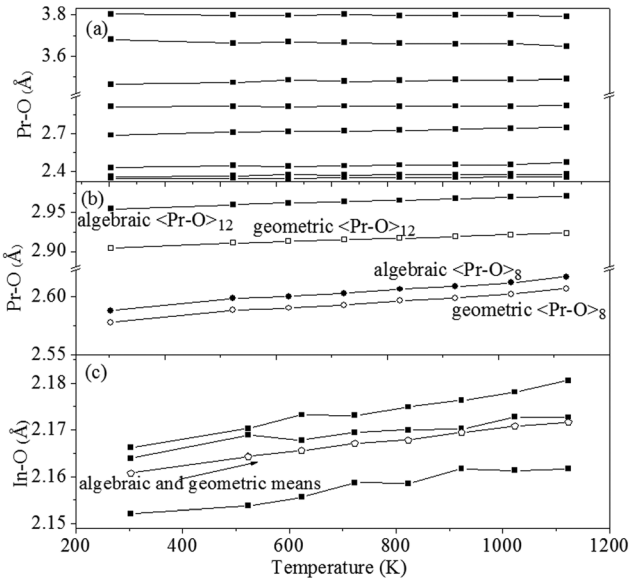

Fig. 2 (a) Temperature evolution of Pr–O interatomic distances in $PrInO_3$. (b) Temperature evolution of the algebraic and geometric averages of the Pr–O interatomic distances calculated using 8 and 12 coordinated Pr. (c) Temperature evolution of the individual and average In–O distances in $PrInO_3$.

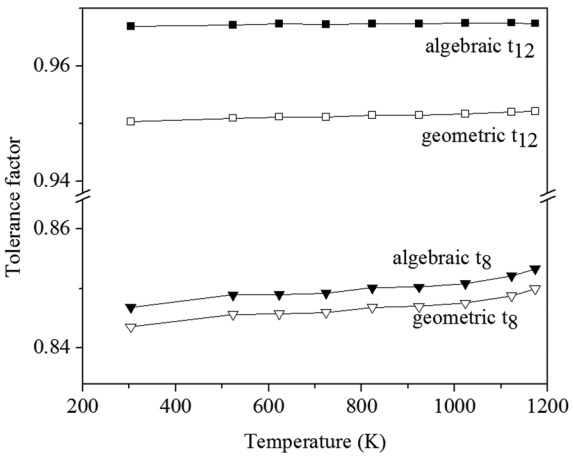

Fig. 3 Temperature dependence of the tolerance factor calculated using algebraic and geometrical averaging of the <Pr–O> (in 8 and 12 coordination) and <In–O> interatomic distances in $PrInO_3$.

Corresponding to the slow increase of the mean <In–O> and <Pr–O> bonds, the tolerance factors increase very slightly with temperature in the whole range investigated, with the geometrical tolerance factor calculated for the 12-fold coordinated Pr increasing somewhat faster than the algebraic one. Again regardless of the method of averaging the 8-fold coordinated Pr bonds the calculated tolerance factors remain almost identical.

The temperature dependence of the bond-length distortion calculated for the $PrInO_3$ structure is shown in Fig. 4. The

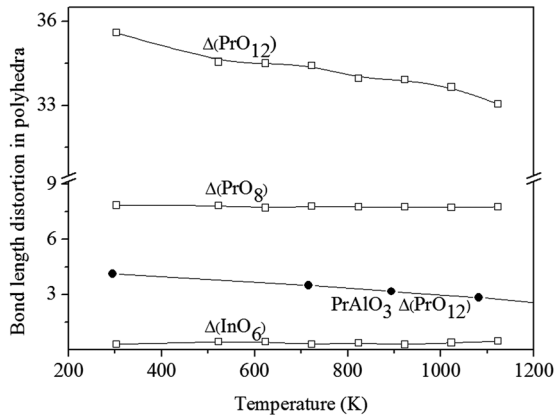

Fig. 4 Temperature dependence of the bond-length distortion in PrO_n (n = 12, 8) and InO_6 polyhedra for $PrInO_3$. The temperature dependence of the bond-length distortion in PrO_{12} for $PrAlO_3$ is shown as solid circles.

bond-length distortion $\Delta(PrO)_8$ calculated for PrO_8 polyhedra is almost constant or slightly increasing with temperature indicating falsely a slight tendency for an increase of the $PrInO_3$ structure distortion. The bond-length distortion $\Delta(PrO)_{12}$ calculated for PrO_{12} polyhedra decreases from ~36 at room temperature to ~33 at 1123 K showing correctly the decrease of structure distortion. This decrease is a result of the slight decrease of the three longest Pr–O bonds with increasing temperature.

The temperature dependence of the Pr and In bond valence sums, as well as the global instability index are shown in Fig. 5. In order to calculate the temperature dependent bond valence parameters $R_0{}^T$ we used $R_0{}^T = R_0 + \left(\frac{dR}{dT}\right)\Delta T$ equation (where $\frac{dR}{dT}(\mathrm{In}) = 0.000015\ \text{Å K}^{-1}$, $\frac{dR}{dT}(\mathrm{Pr}) = 0.000045\ \text{Å K}^{-1}$ and ΔT is the temperature difference from 298 K) reported by Brown *et al.*[36] From this figure it can be concluded that the bond-valence sum for In ions is close to the ideal valence 3 at room temperature and remains nearly constant in the whole investigated temperature range. On the other hand the bond-valence sum for Pr ions increases from 2.88 at room temperature to 2.98 at 1123 K. Consequently the global instability index GII decreases from 0.077 to 0.051.

Neutron diffraction data provide reliable data for calculation of the interatomic bond angles. Table 2 includes the important individual as well as the mean M–O–M bond angles, which are a direct measure of distortion from the cubic perovskite structure caused by rotation and tilting of the almost rigid MO_6 octahedra. These bond angles are also of critical importance for description of electron hopping and virtual charge transfer as well as magnetic exchange interactions in perovskites. In Fig. 6 we show the dependence of t_{12}, $\Delta(PrO)_{12}$, and GII as a function of $\cos^2\langle$M–O–M$\rangle$. The nearly linear relationship between t_{12} and $\Delta(PrO)_{12}$ and $\cos^2\langle$M–O–M$\rangle$ is shown in the figure.

The global instability index also decreases with the increase of $\cos^2\langle$M–O–M$\rangle$ although not quite smoothly. Extrapolation of the linear dependence of the tolerance factor t_{12} calculated for the 12-fold coordinated Pr on $\cos^2\langle$M–O–M$\rangle$ to t_{12} = 1 (to cubic structure) corresponds to $\cos^2\langle$M–O–M$\rangle \approx 1.05$, which is close to the expected In–O–In bond angle 180°. Similar extrapolation of the $\Delta(PrO)_{12}$ dependence on $\cos^2\langle$M–O–M$\rangle$ shows that the bond-length distortion calculated for PrO_{12} polyhedra reaches zero at $\cos^2\langle$M–O–M$\rangle \approx 0.83$, which corresponds to an unreasonable In–O–In bond angle of ~156°.

By comparing the above methods defining distortion of $PrInO_3$ it appears that the tolerance factor calculated for the

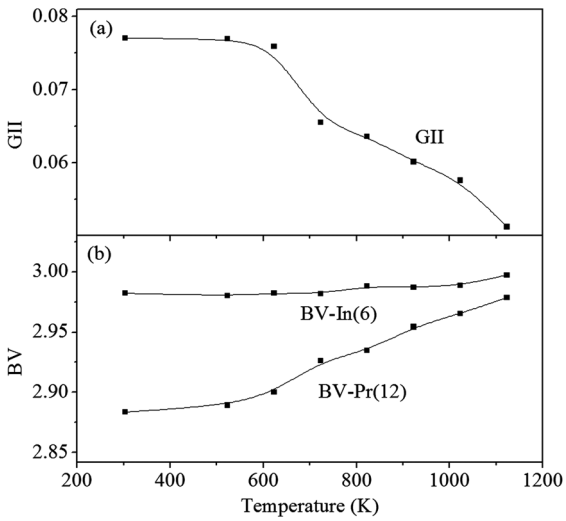

Fig. 5 Temperature dependence of the global instability index (GII) (a) and the Pr and In bond valence sums (BV) (b) for $PrInO_3$.

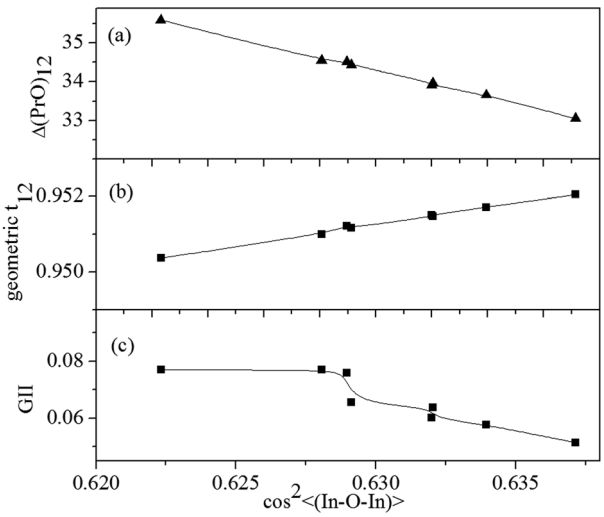

Fig. 6 Bond-length distortion ($\Delta(PrO)_{12}$) (a), tolerance factor (t_{12}) calculated for the 12-fold coordinated Pr (b), and the global instability index (GII) (c) *versus* $\cos^2\langle$In–O–In$\rangle$.

12-fold coordinated Pr by geometrical averaging gives the most reliable and readily measurable results. It is surprising however that the $PrInO_3$, which is severely distorted at room temperature, evolves remarkably slowly with temperature towards the more symmetric phase with smaller distortion.

Comparison of the crystal structure of $PrInO_3$ with other perovskites at room temperature

Comparison of the selected room temperature structural parameters observed in $PrInO_3$ with less distorted perovskite structures of $PrAlO_3$ and $PrGaO_3$ is shown in Table 2. From this table it is clearly seen how an increase of the M ionic radii reduces the symmetry of the Pr-site cation coordination environment and results in an increased variance of the Pr–O bond lengths. In the rhombohedral $PrAlO_3$ phase the 12 oxygen atoms surrounding the Pr separate into three groups, three short bonds of 2.442 Å, six medium bonds of 2.665 Å and three long bonds of 2.891 Å. This variance of the Pr–O bond lengths would suggest that the coordination number of Pr in $PrAlO_3$ is nine (or three). The difference of individual Pr–O bond lengths is approximately 18%. Larger differences of the Pr–O bond lengths (~38%) are observed for the orthorhombic $PrGaO_3$ structure, for which the individual Pr–O bonds are distributed into two groups: eight short bonds of 2.371–2.727 Å and four long bonds of 3.056–3.277 Å. Vasylechko *et al.*[19] concluded from the distribution of Pr–O interatomic distances that the coordination number of Pr in $PrGaO_3$ should be eight. In a more distorted structure of praseodymium $PrInO_3$ the individual Pr–O bonds show increasingly larger differences in lengths (~60%) and different splitting of bond lengths, which would suggest that the coordination number of Pr is eight (or six).

Table 2 shows tolerance factors calculated using reported Pr–O and M–O (M = Al,[18] Ga,[19] In) interatomic distances for $PrMO_3$ perovskites. Based on interatomic distances with 12- and 6-coordination for the Pr and M sites, respectively, the tolerance factors obtained by algebraic averaging are close to 1; t_{12} = 0.9947, 0.9848, and 0.9669 for $PrAlO_3$, $PrGaO_3$ and $PrInO_3$, respectively. The tolerance factors obtained by geometrical averaging are t_{12} = 0.9929, 0.9781 and 0.9504, respectively, and they again better express the effects of increasing crystal structure distortion. On the other hand, the use of the 8-coordination for the Pr site reduces immensely the tolerance factor, indicating incorrectly huge distortion for both the $PrGaO_3$ and $PrInO_3$.

The calculated Pr polyhedral distortion is much more significant in $PrInO_3$ than in $PrGaO_3$ and $PrAlO_3$ with $\Delta(PrO)_{12}$ values of ~36, 13.9 and 4.1, respectively. When the four longest Pr–O bonds are removed from the Pr coordination polyhedron a much more symmetric 8-coordinated Pr environment is obtained, which can be compared with other studied orthorhombic perovskites. The observed $\Delta(PrO)_8$ = 7.9 in the $PrInO_3$ structure is quite large, almost three times larger than $Ä(PrO)_8$ in $PrGaO_3$, twice larger than that reported for the Ln-orthoferrites[37] and similar to $Ä(LnO)_8$ found for high-pressure synthesized lanthanide scandates (Ln = Gd, Tb, Dy, Ho).[37]

Bond-valence sums are shown in Table 4 for Pr and M ions within the PrO_8, PrO_{10}, PrO_{12} and MO_6 (M = Al, Ga, In) polyhedra. From these values large differences in Pr–O bond strengths in $PrMO_3$ structures are obtained as shown in Table 3a–c. The valence sums of 12-coordinated Pr^{+3} are decreasing from 3.16 in $PrAlO_3$ to 2.88 in $PrInO_3$. These values imply that Pr–O bonds are under moderate compressive stress in $PrAlO_3$ and $PrGaO_3$ and under small tensile stress in $PrInO_3$. The valence sums of 6-coordinated M^{+3} in $PrMO_3$ are also decreasing from 3.10 for $PrAlO_3$ to 2.98 for $PrInO_3$. However, deviations from the ideal valence 3 are not large especially for Ga and In. The Al in $PrAlO_3$ is unexpectedly overbonded indicating that Al–O bonds are under compressive stress (Table 3c and Table 4). While the decreasing value of the valence sums of the 12-coordinated Pr^{+3} is expected in general for the perovskites with the decreasing tolerance factor $t < 1$, the decreasing value of the valence sums of the 6-coordinated M^{+3} is unexpected. The discrepancy factors for Al and Pr in $PrAlO_3$ are especially unusual since both are positive although a mixture of overbonded and underbonded ions is expected for steric strains.

The main drawback of the bond valence method is manifested here, namely its highly parameterized nature. Bond valences (bond strengths) are calculated using tabulated bond-valence parameters R_0 determined empirically for each bond type. We used parameters given by Brese and O'Keefe[38] for all $PrMO_3$ compounds. Parameters R_0 reported by Brown[39] are the same for Pr–O, In–O and Ga–O but different for Al–O. If we use R_0 = 1.620 Å from ref. 39 rather than the value of R_0 = 1.644 Å from ref. 38 the discrepancy factor for Al^{3+} would change from +0.1 to −0.15 implying correctly the tensile stress for the Al–O bonds. Regardless of the R_0 parameter chosen for Al the global instability indices GII decreased from 0.12 (R_0 from ref. 38) and 0.11 (R_0 from ref. 39) for the less distorted $PrAlO_3$ to 0.07 and 0.077 for the more distorted structures of $PrGaO_3$ and $PrInO_3$ respectively. This may occur when the structural stresses are induced as the M ion becomes larger and are successfully relieved by tilting and distortion of the octahedral units permitted in the space group *Pnma*.

Comparison of the crystal structure of $PrInO_3$ with other perovskites at variable temperatures

Comparing the temperature dependence of the tolerance factors demonstrated for $PrGaO_3$ in Fig. 7 in ref. 19 with that calculated for $PrInO_3$ (see Fig. 3) it is apparent that t_{obs} for $PrGaO_3$ increases faster, indicating a faster decrease of the perovskite structure distortion. Vasylechko *et al.*[19] observed that the decrease of distortion with the increase of temperature is caused by a systematic increase of 8 shortest Pr–O distances and a decrease of 4 longest distances for $PrGaO_3$. These changes motivated him to assign an increased Pr coordination number from eight to ten for temperatures higher than 1000 K. For the less distorted $PrAlO_3$ an increase in temperature leads to a systematic increase of three shortest and a decrease of three longest Pr–O distances whereas six medium Pr–O interatomic distances remain nearly constant. Conse-

quently, around ~1800 K all Pr–O bonds become equal and the rhombohedral structure transforms to the cubic perovskite structure.

The bond-length distortion calculations of $\Delta(PrO)_{12}$–$\Delta(PrO)_8$ for $PrMO_3$ structures (M = Al, Ga and In) show a similar trend to the tolerance factor. For $PrAlO_3$ and $PrGaO_3$ there is a visible tendency for a decrease of the bond-length distortion calculated for PrO_8–PrO_{12} polyhedra with increasing temperature leading to a more symmetrical coordination of Pr and consequently to a decrease of the perovskite structure deformation. It is most distinct for the less distorted rhombohedral $PrAlO_3$ where the value of the bond-length distortion $\Delta(PrO)_9$ and $\Delta(PrO)_{12}$ decreases with temperature from ~1.6 to 4, respectively towards zero as expected for the regular coordination of the cubic structure (Fig. 4). For $PrGaO_3$ the bond-length distortion $\Delta(PrO)_{12}$ decreases from ~18 at room temperature to ~14 at 1000 K (see Fig. 8 in ref. 19). In the same temperature range bond-length distortion $\Delta(PrO)_{12}$ in $PrInO_3$ decreases only from ~36 to ~34 indicating a much smaller tendency for a decrease of the structure deformation (Fig. 4).

It is valuable to compare the slow decrease of $PrInO_3$ structure distortion with temperature with other $(A/R)MO_3$ perovskites, which contain other ions rather than Pr and In on the A/R- and M-sites, respectively. As discussed in previous chapters there are several methods used in order to describe and quantify distortion in the ideal perovskite structure. We have shown that several coordination numbers can be used for these methods leading to inconsistency and problems to compare perovskites with different degrees of distortion from the cubic structure. We believe that the geometrical tolerance factor $t_{12}(T)$ calculated using ideal 12-fold coordinated A-sites can be consistently and effectively used, especially when the structures with different degrees of distortion are compared. Geometrical averaging is necessary to diminish the too large contribution of the longest bonds as is carried out by algebraic averaging. This approach is to some degrees similar to the bond valence method, which also uses 12-fold coordinated A-sites and exponential averaging to diminish the contribution of the longest bonds to the total charge of ions.

Comparisons of the $t_{12}(T)$ calculated using data obtained from the Inorganic Crystal Structure Database (ICSD) for two groups of perovskites are presented in Fig. 7 (for $A^{3+}M^{3+}O_3$) and Fig. 8 (for $A^{2+}M^{4+}O_3$).[40–49]

Unfortunately the number of examined compounds was restricted by the requirement of the availability of reliable NPD data as a function of temperature. The division of perovskite into two groups is a consequence of different dependences of $t_{12}(T)$ on the temperature. Fig. 7 shows the notably slow decrease of the structure distortion as evident by the slow increase of $t_{12}(T)$ with temperature. The heavily distorted $PrInO_3$ studied here conforms well to the observed tendency. The $A^{2+}M^{4+}O_3$ perovskites exhibit much faster reduction of structure distortion with increasing temperature (see Fig. 8).

The dependence of the thermal behavior on the bond strength z/p, where z is the cation charge and p is the cation coordination, was studied by Megaw[50] and extended by Hazen

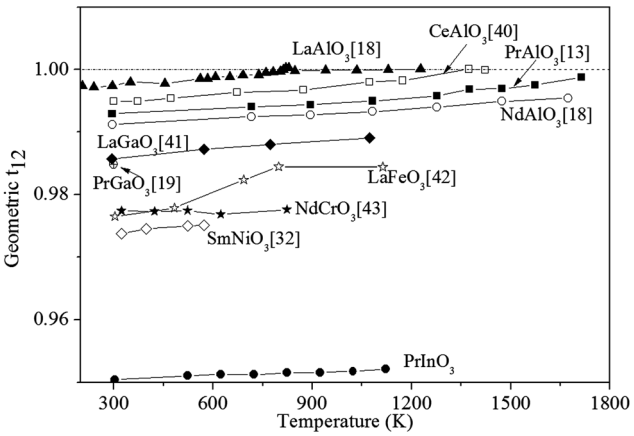

Fig. 7 Temperature dependence of the tolerance factor t_{12} calculated by geometric averaging of the average <A–O> bond length using data obtained from the Inorganic Crystal Structure Database (ICSD) for the $A^{3+}M^{3+}O_3$ perovskites. The horizontal dash-dotted line at t = 1 separates the distorted and ideal cubic structure ranges.

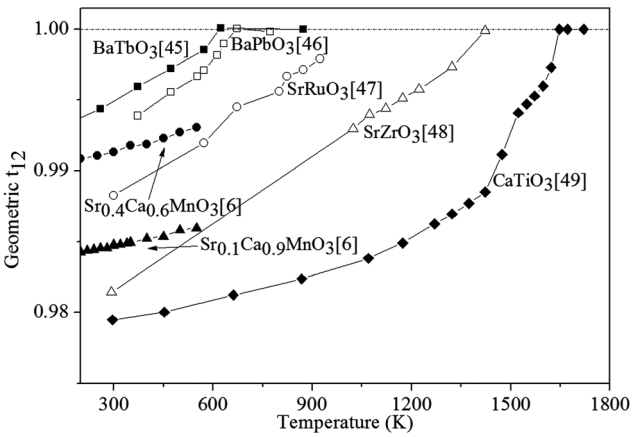

Fig. 8 Temperature dependence of the tolerance factor t_{12} calculated by geometric averaging of the average <A–O> bond length using data obtained from the Inorganic Crystal Structure Database (ICSD) for the $A^{2+}M^{4+}O_3$ perovskites. The horizontal dash-dotted line at t = 1 separates the distorted and ideal cubic structure ranges.

and Prewitt,[51] who defined the mean thermal expansion coefficient $\bar{\alpha} = 32.9\left(0.75 - \frac{z}{p}\right) \times 10^{-6}\,^{\circ}C^{-1}$).[39] A direct consequence of their empirical formula is that the metal–oxygen bonds with cations of the same charge and coordination should have approximately the same expansion rate. This relationship supports the observed differences of the temperature evolution of the tolerance factor $t_{12}(T)$ depending on the formal charge of the A and M cations.

The mean expansion coefficient for the 12-coordinated A^{+2} and 6-coordinated M^{+4} cations is close to 19×10^{-6} and 3×10^{-6}, respectively, leading to the ratio of expansivities of the AO_{12} to MO_6 bonds close to 6 in the group of $A^{2+}B^{4+}O_3$ perovskites. For the $A^{3+}B^{3+}O_3$ perovskites this ratio is three times lower, because mean expansion coefficients for 12- and 6-co-

ordinated A^{+3} and M^{+3} ions are approximately close to 16×10^{-6} and 8×10^{-6}, respectively. The higher ratio of the expansivities of the AO_{12} to MO_6 bonds in $A^{2+}M^{4+}O_3$ than in the $A^{3+}M^{3+}O_3$ group of perovskites results in a faster increase of the tolerance factor with temperature.

Moreover, in both groups, the decreasing coordination number of the A ion with increasing perovskite structure distortion should be taken into account. In the most heavily distorted compounds the smaller expansivity of the highly irregular AO_{12} polyhedron with the reduced number of short A–O bonds is expected, and consequently the slower increase of $t_{12}(T)$ with temperature. This explains why the expansivities of the InO_6 and PrO_{12} in $PrInO_3$ are well-matched causing a notably slow decrease of the structure distortion.

Conclusions

In summary, by using high-resolution neutron-powder diffraction we have studied structural properties of the $PrInO_3$ in the temperature range 303–1123 K. We have found that $PrInO_3$ has a distorted orthorhombic $GdFeO_3$-type structure in the whole temperature range. The bond length and bond-angle analysis revealed a very slow temperature decrease of structure distortion in the ideal cubic perovskite as measured by various measurement methods. By comparing results obtained by global instability index, bond-length distortion, and tolerance factor methods for similar perovskites $PrAlO_3$ and $PrGaO_3$ we concluded that the most reliable parameter describing temperature-dependent properties is the tolerance factor t_{12} based on geometrical averaging of the Pr–O interatomic distances and calculated for the 12-fold coordinated Pr. The additional advantage of the tolerance factor method results from the possibility to extend it to predict the average structural distortion and the geometrical stability of the perovskites at various temperatures once the accurate dependence of $t(x,T,d)$ on T and d is found.

The structure distortion in $PrInO_3$ has also been compared with other AMO_3 perovskites with ions in the fixed oxidation state on the A and M crystal sites. We have found that the $A^{3+}M^{3+}O_3$ perovskites exhibit a much slower thermal change of structural distortion and the tolerance factor t_{12} than the $A^{2+}M^{4+}O_3$. This is consistent with the Hazen and Prewitt thermal expansion coefficient based on the bond strength z/p calculation.

Comparison with perovskites containing mixed-valent ions, which allows for a wide range of changes of the tolerance factor as a function of oxygen content $t_{12}(T,d)$ in AMO_{3-d}, demonstrates much less flexibility for changing the solubility ranges and structures of the AMO_3 perovskites. This flexibility is further reduced for the $A^{3+}M^{3+}O_3$ perovskites like $PrInO_3$, for which even a substantial change of the synthesis temperature has a minor effect on controlling the resulting $t_{12}(T)$ and the structural phase. The only parameter left for these materials is the total pressure, which may significantly change $t_{12}(T,P)$ allowing controlled formation of various perovskite and hexagonal phases.

Acknowledgements

Work at the Department of Mechanics, Materials Science and Engineering was supported by the Wroclaw University of Technology under contract no. S40135. Work at NIU was supported by The Institute for Nanoscience, Engineering, and Technology – InSET.

References

1 I. A. Abdel-Latif, *J. Phys.*, 2012, **1**(3), 15.
2 M. A. Pena and J. L. G. Fierro, *Chem. Rev.*, 2001, **101**, 1981.
3 L. Vasylechko, A. Senyshyn and U. Bismayer, *Handbook on the Physics and Chemistry of Rare Earths*, 2009, vol. 39, p. 113.
4 A. Kudo and Y. Miseki, *Chem. Soc. Rev.*, 2009, **38**, 253.
5 J. Sato, S. Saito, H. Nishiyama and Y. Inoue, *J. Phys. Chem.*, 2003, **107**, 7975.
6 B. Dabrowski, O. Chmaissem, M. Mais, S. Kolesnik, J. D. Jorgensen and S. Short, *J. Solid State Chem.*, 2003, **170**, 154.
7 S. Remsen, B. Dabrowski, O. Chmaissem, J. Mais and A. Szewczyk, *J. Solid State Chem.*, 2011, **184**, 2306.
8 O. Chmaissem, B. Dabrowski, S. Kolesnik, J. Mais, D. E. Brown, R. Kruk, P. Prior, B. Pyles and J. D. Jorgensen, *Phys. Rev. B: Condens. Matter*, 2001, **64**, 134412.
9 R. D. Shannon, *Acta Crystallogr., Sect. A: Cryst. Phys., Diffr., Theor. Gen. Cryst.*, 1976, **32**, 751.
10 B. Dabrowski, O. Chmaissem, J. Mais and S. Kolesnik, *Acta Phys. Pol., A*, 2004, **105**, 45.
11 V. M. Goldschmidt, *Naturwissenschaften*, 1926, **14**, 477.
12 L. Suescun, B. Dabrowski, J. Mais, S. Remsen, J. W. Richardson Jr., E. R. Maxey and J. D. Jorgensen, *Chem. Mater.*, 2008, **20**, 1636.
13 O. Chmaissem, B. Dabrowski, S. Kolesnik, M. Mais, J. D. Jorgensen, S. Short and S. Botez, *Phys. Rev. B: Condens. Matter*, 2005, **72**, 104426.
14 O. Chmaissem, B. Dabrowski, S. Kolesnik and J. Mais, *Phys. Rev. B: Condens. Matter*, 2006, **74**, 144415.
15 D. K. Pratt, J. W. Lynn, J. Mais, O. Chmaissem, D. E. Brown, S. Kolesnik and B. Dabrowski, *Phys. Rev. B: Condens. Matter*, 2014, **90**, 140401(R).
16 C. Abughayada, B. Dabrowski, S. Remsen, S. Kolesnik and O. Chmaissem, *J. Solid State Chem.*, 2014, **217**, 127.
17 R. D. Burbank, *J. Appl. Crystallogr.*, 1970, **3**, 112.
18 C. J. Howard, B. J. Kennedy and B. C. Chakoumakos, *J. Phys.: Condens. Matter*, 2000, **12**, 349.
19 L. Vasylechko, Y. Pivak, A. Senyshyn, D. Savytskii, M. Berkowski, H. Borrmann, M. Knapp and C. Paulmann, *J. Solid State Chem.*, 2005, **178**, 270.

20 J. L. Bates, C. W. Griffin and W. J. Weber, NASA STI/Recon Technical Report N, 1988, 89, 11310.
21 E. Cohen, L. A. Risberg, W. A. Nordland, R. D. Burbank, R. C. Sherwood and L. G. Van Uitert, *Phys. Rev.*, 1969, **186**, 476.
22 R. T. Harley, W. Hayes, A. M. Perry and S. R. P. Smith, *J. Phys. C: Solid State Phys.*, 1973, **6**, 2382.
23 R. J. Birgeneau, J. K. Kjems, G. Shirane and L. G. Van Uitert, *Phys. Rev. B: Solid State*, 1974, **10**, 2512.
24 J. Richter, *Mixed Conducting Ceramics for High Temperature Electrochemical Devices*, Ph.D. dissertation, ETH Zurich, 2008.
25 I. D. Brown, *Structure and Bonding*, Springer-Verlag, 1981, p. 2.
26 I. D. Brown, *Z. Kristallogr.*, 1992, **199**, 255.
27 B. H. Toby, *J. Appl. Crystallogr.*, 2001, **34**, 210.
28 S. Sasaki, C. T. Prewitt and R. C. Liebermann, *Am. Mineral.*, 1983, **68**, 1189.
29 J. A. Alonso, M. J. Martínez-Lope, M. T. Casais and M. Fernández-Díaz, *Inorg. Chem.*, 2000, **39**, 917.
30 Y. Wang, Y. Sui, P. Ren, L. Wang, X. J. Wang, W. H. Su and H. Fan, *J. Inorg. Chem.*, 2010, **49**, 321.
31 B. Veličkov, V. Kahlenberg, R. Bertram and M. Bernhagen, *Z. Kristallogr.*, 2007, **222.9**, 466.
32 G. Mather, F. Figueiredo, J. Rom and S. Garcia-Martın, *Inorg. Chem.*, 2008, **47**, 921.
33 K. H. Ahn, T. Lookman and A. R. Bishop, *Nature*, 2004, **428**, 401.
34 F. W. Lytle, *J. Appl. Phys.*, 1964, **35**, 2212.
35 Y. Zhao, D. J. Weidner, J. B. Parise and D. E. Cox, *Phys. Earth Planet. Inter.*, 1993, **76**(1–2), 1.
36 I. D. Brown, A. Dabkowski and A. McCleary, *Acta Crystallogr.*, 1997, 750.
37 R. P. Liferovich and R. H. Mitchell, *J. Solid State Chem.*, 2004, **177**, 2188.
38 N. E. Brese and M. O'Keefe, *Acta Crystallogr., Sect. B: Struct. Sci.*, 1991, **47**, 192.
39 I. D. Brown, *Private communication*; http://www.ccp14.ac.uk/ccp/web-mirrors/i_d_brown/.
40 W. T. Fu and D. J. W. IJdo, *J. Solid State Chem.*, 2004, **177**(4–5), 1667.
41 W. Martit, P. Fischert, F. Altorferj, H. J. Sheel and M. Tadin, *J. Phys.: Condens. Matter*, 1994, **6**, 127.
42 S. M. Selbach, J. R. Tolchard, A. Fossdal and T. Grande, *J. Solid State Chem.*, 2012, **196**, 249.
43 M. W. Lufaso, S. J. Mugavero III, W. R. Gemmill, Y. Lee, T. Vogt and H.-C. zur Loye, *J. Alloys Compd.*, 2007, 433.
44 P. F. Henry, M. T. Weller and C. C. Wilson, *Chem. Mater.*, 2002, **14**(10), 4104.
45 W. T. Fu, D. Visser, K. S. Knight and D. J. W. IJdo, *J. Solid State Chem.*, 2004, **177**(4–5), 1667.
46 W. T. Fu, D. Visser, K. S. Knight and D. J. W. IJdo, *J. Solid State Chem.*, 2007, **180**(5), 1559.
47 J. S. Gardner, G. Balakrishnan and D. M.K. Paul, *Physica C*, 1995, **252**(10), 303; B. J. Kennedy and B. A. Hunter, *Phys. Rev. B: Condens. Matter*, 1998, **58**(2), 653.
48 B. J. Kennedy, C. J. Howard and B. C. Chakoumakos, *Phys. Rev. B: Condens. Matter*, 1999, **59**, 4023.
49 R. Ali and M. Yashima, *J. Solid State Chem.*, 2005, **178**(9), 2867.
50 H. D. Megaw, *Mater. Res. Bull.*, 1971, **6**, 1007.
51 R. M. Hazen and C. T. Prewitt, *Am. Mineral.*, 1977, **62**, 309.